Phonon scattering of interfacial strain field between dissimilar lattices

Qingping Meng,[1,2] Lijun Wu,[1] and Yimei Zhu[1,*]
[1]*Brookhaven National Laboratory, Upton, New York 11973, USA*
[2]*School of Materials Science and Engineering, Shanghai Jiao Tong University, Shanghai 200030, China*
(Received 13 November 2012; published 8 February 2013)

Interfaces play a crucial role in controlling the thermal conductivity of a material, as evidenced by the major ongoing research in nanoscale precipitation engineering to improve the performance of thermoelectric materials. To understand their influence on phonon scattering, and thus thermal conductivity, we explored the effect of interfacial strain fields (ISFs) on interfaces with a different misfit between the two dissimilar lattices comprising the interface. We found that phonon scattering depends strongly on the frequency of the incident phonon wave; phonons with frequencies below a critical value pass transparently through the strain zone of the interfaces. Our calculations suggest that the classical acoustic mismatch model (AMM) and the diffusive mismatch model (DMM) represent the two extreme limits of phonon scattering, and that, in reality, scattering lies between these limits. For long-wavelength (low-frequency) phonons, the AMM adequately describes the thermal conductivity of the interfaces. As the frequency of the incident phonons increases, phonon scattering becomes progressively more diffuse to the point where the DMM represents the dominant mechanism for thermal conductivity. Furthermore, we noted that phonon scattering from the interfacial strain field can lower thermal conductivity effectively at high temperatures. We discuss the implications of our findings in explaining the experimental observations of thermal conductivity across precipitates and grain boundaries in thermoelectric materials.

DOI: 10.1103/PhysRevB.87.064102 PACS number(s): 63.20.kp, 66.70.−f, 68.35.−p

I. INTRODUCTION

Thermal conductivities across interfaces recently have attracted increasing attention due to their importance in various applications, including solar panels, cooling microelectronics, and thermoelectric devices that convert waste heat to electricity. In some cases, such as computer processors, heat must be removed as quickly and efficiently as possible, while in other devices, such as thermoelectric ones, heat transfer should be as slow as possible.[1] Thermal conductivity across interfaces is an important element that affects heat transport in these devices. The thermal resistance of interfaces first was observed between metal and liquid helium[2] but later was seen also at the interface between two solids.[2] Two theoretical frameworks are used to estimate the thermal resistance of the interfaces: the acoustic mismatch model (AMM),[3] and the diffuse mismatch model (DMM).[4,5] In the former, the two media are regarded as two elastic continua, and, hence, the interface junction between them displays no lattice match; phonon propagation at the interface is similar to photon propagation. When a phonon impinges on the interface, it has a certain probability of being reflected or transmitted, and the angle is determined by the acoustic analog of Snell's law.[3] On the other hand, the DMM assumes that all incident phonons are diffusively scattered at the interface. Scattered phonons have an energy proportional to the available density of states of the material on each side of the interface. Besides applying AMM and DMM, other researchers have applied lattice dynamics[6–11] in their simulations, wherein two crystals with different atomic masses and force constants are joined at the interface. These theoretical models and lattice-dynamical simulations work well at low temperatures, but at high temperatures, the experimentally determined resistance of the thermal boundary differs significantly from the theoretical predictions. The discrepancy may reflect additional scattering from the strain field induced by the interface. So far, all the existing models and simulations rest upon the assumption that there is no interfacial lattice distortion and strain. Although Pettersson and Mahan[11] investigated thermal conductance between two crystals with a different lattice constant, their calculations did not encompass the effects of interfacial lattice misfit and strain.

Strain associated with crystalline defects strongly affects the lattice's thermal conductivity.[12,13] Carruthers[13] detailed phonon scattering from various defects, suggesting that such scattering depends strongly on the distribution of the induced lattice displacement from defects. Different types of crystalline defects have a different frequency (ω) dependence for phonon relaxation time $\tau(\omega)$, as well as temperature (T) dependence of thermal conductivity $\kappa(T)$. For example, the relationship between displacement, $\mathbf{V}$, of a spherical point defect and position, $\mathbf{r}$, is $\mathbf{V}(\mathbf{r}) \propto r^{-2}$ (Ref. 14), yielding $\tau(\omega)^{-1} \propto \omega^4$ and $\kappa(T) \propto T^{-1}$; for an F-center point defect, the displacement is $\mathbf{V}(\mathbf{r}) \propto r^{-1}$ (Ref. 13), yielding $\tau^{-1} \propto \omega^2$ and $\kappa(T) \propto T$. This signifies that the variation in temperature of thermal conductivity can reflect the difference in lattice displacements associated the different types of point defects.

The interfacial strain field (ISF) substantially alters the elastic modulus of multilayered thin films,[15] the domain structure of ferroelectrics and ferroelastic films,[16,17] and the band gap and the effective masses of the holes and electrons of semiconductor multilayered devices.[18] Although some researchers have speculated that an ISF may decrease thermal conductivity,[5] the details never have been reported. In this paper, we address phonon-scattering behavior from the ISF based on Carruthers' theory[13] and discuss the influence of

various ISFs on phonon scattering and interfacial thermal conductivity.

II. FORMALISM

A. Relaxation time for the phonon strain field scattering process

Following Carruthers,[13] the Hamiltonian of a crystal containing a strain field is written as

$$H = H_0 + H_p, \tag{1}$$

where H_0 is the Hamiltonian of the crystal in the harmonic approximation, and H_p is the perturbation Hamiltonian arising from the strain field. H_0 is expressed as

$$H_0 = \sum_{\mathbf{m},\alpha} \frac{p_\alpha^2(\mathbf{m})}{2M(\mathbf{m})} + \sum_{\substack{\mathbf{m},\mathbf{n}\\ \alpha,\beta}} \Phi_{\alpha,\beta}(\mathbf{m},\mathbf{n}) u_\alpha(\mathbf{m}) u_\beta(\mathbf{n}). \tag{2}$$

The first term is the kinetic energy; $M(\mathbf{m})$ is the atomic mass at the equilibrium lattice site, $\mathbf{m}$; $p_\alpha(\mathbf{m})$ and $u_\alpha(\mathbf{m})$, respectively, are the α component of the momentum and the displacement of that atom, and $\Phi_{\alpha,\beta}(\mathbf{m},\mathbf{n})$ is the second-order harmonic force constant.

We carried out the transformation to the creation and destruction operators given by

$$\mathbf{u}(\mathbf{m}) = \sum_{\mathbf{q},\lambda} \left(\frac{\hbar}{2\rho\Omega\omega_{\mathbf{q}\lambda}}\right)^{\frac{1}{2}} [a_{\mathbf{q}\lambda} \exp(i\mathbf{q}\cdot\mathbf{m}) + a^*_{\mathbf{q}\lambda} \exp(-i\mathbf{q}\cdot\mathbf{m})]\mathbf{e}_{\mathbf{q}\lambda}, \tag{3}$$

where the sum on the wave vector $\mathbf{q}$ goes over the first Brillouin zone; $\omega_{\mathbf{q}\lambda}$ is the phonon frequency with wave vector $\mathbf{q}$ and polarization index λ; $\mathbf{e}_{\mathbf{q}\lambda}$ represents the polarization vector; ρ is the density of the crystal; and Ω is the total volume. Hereafter, we write q for representing the pair of variables $\mathbf{q}$, λ. Here, a_q and a_q^*, respectively, are the phonon creation and annihilation operators that follow the commutation relations:

$$[a_q, a^*_{q'}] = \Delta(\mathbf{q}-\mathbf{q}')\delta_{\lambda\lambda'} \tag{4a}$$

and

$$[a_q, a_{q'}] = [a_q^*, a_{q'}^*] = 0. \tag{4b}$$

Using Eqs. (3) and (4), expression (1) becomes

$$H_0 = \sum_q \hbar\omega_q \left(a_q^* a_q + \frac{1}{2}\right). \tag{5}$$

The perturbation Hamiltonian H_p is written as[13]

$$H_p = \frac{\hbar}{4\rho\Omega} \sum_{\substack{qq'\\ ijk}} (\omega_q\omega_{q'})^{-\frac{1}{2}} e_q^j e_{q'}^k \times [a_q a^*_{q'} V^i_{q'-q} b_{ijk}(q,q',q-q') + \text{H.c.}], \tag{6}$$

where V_q is a coefficient of the Fourier series of strain displacement, and $b_{ijk}(q,q',q-q')$ is defined as

$$b_{ijk}(q,q',q-q') = \sum_{mn} B^{ijk}_{mn} F_q^* F_{q'} F_{q-q'}, \tag{7}$$

where

$$F_q = \exp(i\mathbf{q}\cdot\mathbf{m}) - \exp(i\mathbf{q}\cdot\mathbf{n}), \tag{8}$$

and B^{ijk}_{mn} is the third-order force constant. According to the basic formula of the time-dependent perturbation theory, the probability for a transition from state q to state q' is[13,19]

$$P_{q\to q'} = \frac{2\pi}{\hbar} |\langle\psi_{q'}|H_p|\psi_q\rangle|^2 \delta(E_{q'} - E_q). \tag{9}$$

Using the symmetry properties, the matrix element $M_{q'\to q} = |\langle\psi_{q'}|H_p|\psi_q\rangle|$ for our case is

$$M_{q'\to q} = \frac{\hbar}{2\rho\Omega} C_{q'q} \left[\frac{(N_q+1)N_{q'}}{\omega_{q'}\omega_q}\right]^{\frac{1}{2}}, \tag{10a}$$

and

$$M_{q\to q'} = \frac{\hbar}{2\rho\Omega} C^*_{qq'} \left[\frac{(N_{q'}+1)N_q}{\omega_{q'}\omega_q}\right]^{\frac{1}{2}}, \tag{10b}$$

where

$$C_{qq'} = \sum_{ijk} V^i_{q'-q} e_q^j e_{q'}^k b_{ijk}(q,q',q'-q). \tag{11}$$

The rate of change of the phonon number in state q using the transition probability of Eq. (9) is

$$\frac{dN_q}{dt} = \frac{\pi}{2\rho^2\Omega^2} \sum_{q'} \frac{\delta(\omega_{q'}-\omega_q)}{\omega_q\omega_{q'}} |C_{qq'}|^2 (N_{q'} - N_q). \tag{12}$$

We then can write

$$N_q = N_q^0 + n_q, \tag{13}$$

where n_q is the deviation from the equilibrium distribution N_q^0. Because $N_q^0 = N_{q'}^0$, and assuming $n_{q'} = 0$, i.e., the single-mode approximation,[13] which eliminates the coupling between N_q and $N_{q'}$ in Eq. (12), meaning the rate of change of n_q only depends on n_q, the relaxation time $\tau(q)$ has the relation

$$\frac{1}{\tau(q)} = \frac{\pi}{2\rho^2\Omega^2} \sum_{q'} \frac{\delta(\omega_{q'}-\omega_q)}{\omega_q\omega_{q'}} |C_{qq'}|^2. \tag{14}$$

To simplify our calculation, we consider only the nearest neighbor interaction, and so Carruthers' results[13] can be used

$$B^{ijk}_{mn} = \frac{g a_i a_j a_k}{a^3}, \tag{15}$$

and

$$C_{qq'} = \frac{Ng}{2a^3} \sum_{\mathbf{a}} (\mathbf{V}_{\mathbf{q}'-\mathbf{q}}\cdot\mathbf{a})(\mathbf{e}_{\mathbf{q}}\cdot\mathbf{a})(\mathbf{e}_{\mathbf{q}'}\cdot\mathbf{a})(1-e^{-i\mathbf{q}\cdot\mathbf{a}}) \times (1-e^{i\mathbf{q}'\cdot\mathbf{a}})(1-e^{i(\mathbf{q}'-\mathbf{q})\cdot\mathbf{a}}), \tag{16}$$

where the sum is taken over the nearest neighbors of one atom. Here, a_i is the i component of **a,** and the coefficient g pertains to the macroscopic parameters of elasticity, and the Grüneisen constant, and the like. Herein, our usage of Carruthers' findings is $g \approx 24\gamma\rho c^2$ (γ is Grüneisen constant; c is the velocity of sound). Adopting the acoustic approximation $\omega = cq$,

we have

$$\frac{\delta(\omega_{q'}-\omega_q)}{\omega_q\omega_{q'}}=\frac{1}{c^3}\cdot\frac{\delta(|\mathbf{q}'|-|\mathbf{q}|)}{|\mathbf{q}||\mathbf{q}'|}. \tag{17}$$

Eq. (14) becomes

$$\frac{1}{\tau(q)}=\frac{\pi g^2}{8\rho^2 a^{12}c^3}\sum_{q'}\frac{\delta(|\mathbf{q}'|-|\mathbf{q}|)}{|\mathbf{q}||\mathbf{q}'|}\times\left|\sum_a(\mathbf{V}_{\mathbf{q}-\mathbf{q}'}\cdot\mathbf{a})(\mathbf{e}_{\mathbf{q}}\cdot\mathbf{a})(\mathbf{e}_{\mathbf{q}'}\cdot\mathbf{a})(1-e^{-i\mathbf{q}\cdot\mathbf{a}})\times(1-e^{i\mathbf{q}'\cdot\mathbf{a})}(1-e^{i(\mathbf{q}'-\mathbf{q})}\cdot\mathbf{a})\right|^2. \tag{18}$$

From $\tau(q)$, we obtain the thermal conductivity:

$$\kappa=\sum_q\tau(q)C(\omega_q)c^2, \tag{19}$$

where $C(\omega_q)$ is the heat capacity, and c is the group velocity of the phonon. To assess the influence of the ISF on the thermal conductivity of the interface, we must know the value of displacement related to the ISF and its Fourier components.

B. The displacement related to ISF

Frank and Van der Merwe[20] were the first to study the strain field of the epitaxial layer of a crystal. Van der Merwe[21] developed their theory based on two semi-infinite crystals [Fig. 1(a)]. In it, these two crystals with lattice constants a and b meet in the surface, xoy (the y axis is perpendicular to the plane of the paper), and d is the equilibrium distance between them. The lattice constants of the two crystals have

$$Pb=(P+1)a=\left(P+\tfrac{1}{2}\right)c=p, \tag{20}$$

where P is an integer; p is the distance between the dislocations, which also represents the dissimilarity of the two lattices; and c is the lattice constant of a reference lattice.

According to these conditions, Van der Merwe obtained the displacements related to the ISF of the two crystals[21]

$$u=\pm\frac{c}{2\pi}\arctan\left(\frac{Ae^{\mp Z}\sin X}{1-Ae^{\mp Z}\cos X}\right)-\frac{cZe^{\mp Z}\sin X}{4\pi(1-\sigma)R^2}\quad(x\text{ direction}) \tag{21}$$

and

$$w=\frac{(1-2\sigma)c}{4\pi(1-\sigma)}\ln\left(\frac{R}{1-A}\right)\mp\frac{cAZe^{\mp Z}\left(\cos X-Ae^{\mp Z}\right)}{4\pi(1-\sigma)R^2}\quad(z\text{ direction}) \tag{22}$$

where

$$A=(1+\beta^2)^{\frac{1}{2}}-\beta, \tag{23}$$

and

$$R=(1+A^2e^{\mp 2Z}-2Ae^{\mp Z}\cos X)^{\frac{1}{2}}. \tag{24}$$

The upper and lower signs in Eqs. (21), (22), and (24) refer, respectively to the upper and lower part of the interface, and,

$$X=\frac{2\pi x}{p};\quad Z=\frac{2\pi z}{p}. \tag{25}$$

Here, z is measured from plane S_a for the lower part and S_b for the upper part [see Fig. 1(a)].

$$\beta=\frac{2\pi d}{\mu p}\cdot\frac{1}{\frac{1-\sigma_a}{\mu_a}+\frac{1-\sigma_b}{\mu_b}}, \tag{26}$$

where σ_a, σ_b, μ_a, and μ_b, respectively, denote Poisson's ratio and the shear moduli of the lower- and upper-side lattice, and μ is the effective interfacial shear modulus. u and w, respectively, represent a function with periodic p in the x direction and an exponential fall-off in the z direction. The exponential relationship indicates that the ISF is a short-range strain field, differing from the long-range one of a dislocation. The exponential trend in decrease is determined by the parameter p [see Figs. 1(b) to 1(e)], which represents the dissimilarity of the lattice constants between the two materials making up the interface. The smaller the p value, the larger is the amount of dissimilarity of lattice constants, and, accordingly, the shorter is the range of strain field in the direction normal to the interface [Figs. 1(b) to 1(e)]. The displacement from Eqs. (21) and (22) is associated with a single Peierls-Nabarro dislocation as p tends toward infinity.[21] The Fourier transforms of displacements u and w are

$$u_{\mathbf{q}}=\frac{1}{\Omega}\int u\exp(-i\mathbf{q}\cdot\mathbf{m})d^3\mathbf{m}\quad\text{and}\qquad w_{\mathbf{q}}=\frac{1}{\Omega}\int w\exp(-i\mathbf{q}\cdot\mathbf{m})d^3\mathbf{m}. \tag{27}$$

Using $u_{\mathbf{q}}$ and $w_{\mathbf{q}}$ to replace V_q in Eq. (18), we can calculate the relaxation time of phonon scattering from the ISF.

III. RESULTS AND DISCUSSION

To calculate the relaxation time of phonon scattering, we first must evaluate

$$S=\sum_a(\mathbf{V}_{\mathbf{q}-\mathbf{q}'}\cdot\mathbf{a})(\mathbf{e}_{\mathbf{q}}\cdot\mathbf{a})(\mathbf{e}_{\mathbf{q}'}\cdot\mathbf{a})(1-e^{-i\mathbf{q}\cdot\mathbf{a}})\times(1-e^{i\mathbf{q}'\cdot\mathbf{a}})(1-e^{i(\mathbf{q}'-\mathbf{q})\cdot\mathbf{a}}) \tag{28}$$

in Eq. (18). In this calculation, we fix on one atom and sum over the $\mathbf{a}$'s connecting it to its nearest neighbors; then, using the approximation of nearest neighbor, S for a simple cubic lattice can be written as

$$\begin{aligned}S=u_{q'-q}a^3[&(1-e^{-iq_xa})(1-e^{iq'_xa})(1-e^{i(q'_x-q_x)a})\\&-(1-e^{iq_xa})(1-e^{-iq'_xa})(1-e^{-i(q'_x-q_x)a})]\\&+w_{q'-q}a^3[(1-e^{-iq_za})(1-e^{iq'_za})(1-e^{i(q'_z-q_z)a})\\&-(1-e^{iq_za})(1-e^{-iq'_za})(1-e^{-i(q'_z-q_z)a})].\end{aligned} \tag{29}$$

In the Appendix, we give the S for the other two cubics, viz., the face-center cubic (fcc) and body-center cubic (bcc).

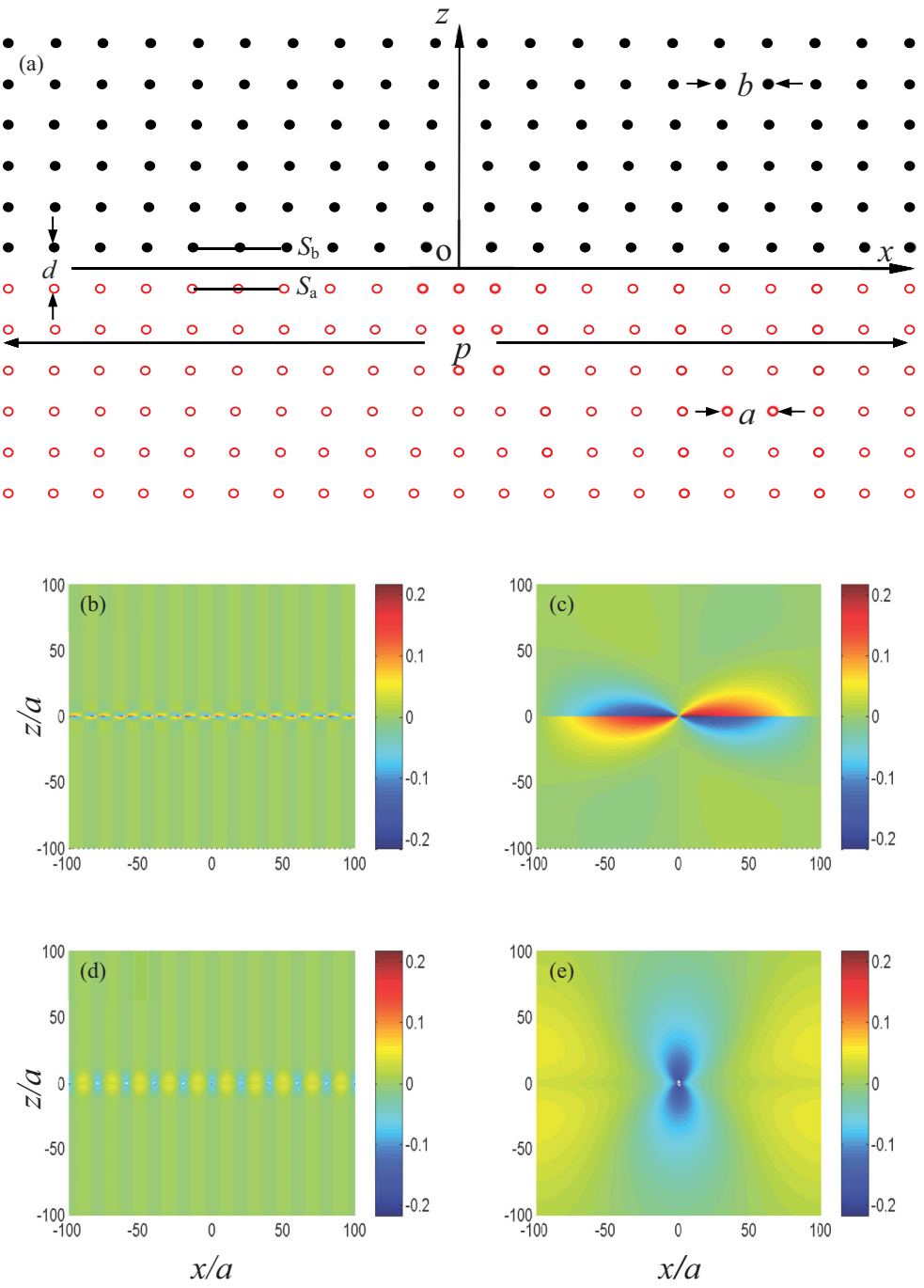

FIG. 1. (Color online) (a) Schematic of the interface between two crystals with different lattice constants. The upper and lower lattices are represented, respectively, by the black solid dots and red circles. Note the displacement u/c of upper part of interface in the x direction for $p = 20a$ (b) and $p = 200a$ (c). Note the displacement w/c in the z direction for the lattice dissimilarity parameter $p = 20a$ (d) and $p = 200a$ (e). (b) to (e) are calculated for shear modulus $\mu = \mu_a = \mu_b$ and Poisson's ratio $\sigma_a = \sigma_b = 0.3$.

Employing a large supercell ensures the accuracy of our calculations because one that is too small will miss many scattering events. However, dealing with a large supercell consumes a great deal of computation time. Hence, in our calculations, we adopted a reasonably sized one, i.e., $1000 \times 1000 \times 1000$, with a periodic boundary condition. Except for the acoustic approximation discussed previously, we used the Debye approximation to determine the distribution of phonon frequency. We selected the Monte-Carlo method for calculating the sum of Eq. (18). We plot our results in Fig. 2; they illustrate the relationship between the inverse of relaxation time and angular frequency with various amounts of dissimilarity in the lattice constants.

Our calculations indicate that there is a critical phonon frequency ω_0 (marked by the arrows in Fig. 2; see Table I). Those phonons for which frequency is lower than the critical value rarely are scattered by the ISF. Figure 2 also shows that the inverse of relaxation time falls abruptly when frequency

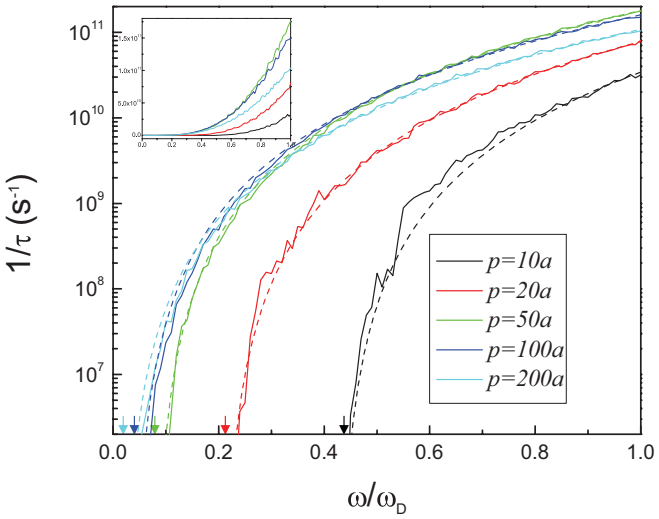

FIG. 2. (Color online) The reverse of phonon relaxation time $(1/\tau)$ versus normalized angular frequency (ω/ω_D) with various misfits (p) at the interface. The arrows point to the ω_o position. ω_D is the Debye frequency. The following are the parameters used in our calculation: Debye temperature is 300 K; the shear moduli on both sides are same; Poisson's ratio is 0.3; the lattice constant is 0.15 nm; and the group velocity of the phonon is 4000 m/s. The number of random points is 2×10^7. The dashed lines are the fitting curves. The inset shows the same relationship as the main figure, but its vertical scale is linear.

decreases to its near critical value, but the critical frequency rises with the decline of the p value. Undoubtedly, this phenomenon originates from the exponential decrease in the range of ISF with the decline in the p value. This finding means that the long-wavelength (low-frequency) phonons, for which wavelength is much larger than the range of ISF, pass transparently through the ISF.

So far, two major approaches have been developed to estimate thermal conductivity across an interface: AMM and DMM. In the former, the interface is treated as a mirror plane. The transmission probabilities are determined by the Fresnel equations. The outcome of the AMM's assumption is that no scattering occurs at the interface.[5] The DMM replaces the assumption of complete specularity in AMM with the opposite extreme: All the phonons are diffusely scattered at the interface.[5] In reality, an interface is neither a simple specular plane, nor a completely rough interface. Rather, it contains an extended strain region that scatters the incident phonons; its thickness determines the frequency range of the scattered phonons. When the wavelength of a phonon is much larger than the thickness of strained region, the thickness scale of ISF is beyond the wave's resolution limit. Then, the strained region appears as a homogeneous effective medium to part of an incident wave. The ISF does not scatter these phonons of long wavelength. Rather, the interface to these phonons resembles a specular plane. Therefore, the AMM model dominates heat transport of the interface for phonons of long wavelength. Conversely, when the wavelength of a phonon is less than the thickness of the strained region of an interface, a homogeneous medium no longer is a valid description; even if the scattering effect is weak locally, over long distances the scattering effect accumulates, and a wave still can be significantly randomized.[22] When that happens, phonon propagation resembles diffusive transport in the ISF. Thus, we can consider the DMM as the main mechanism of thermal transport for phonons of short wavelengths, or high frequencies. The frequency range of the scattering phonons quickly shrinks to a high frequency with a decrease in the thickness of the ISF; the ISF scatters fewer and fewer of the phonons, which only are specularly reflected and refracted by the interface; thereafter, the AMM becomes more important in determining the thermal conductivity of interface. The dominance of the mechanism that defines the interfacial thermal conductivity gradually changes from DMM to AMM with an increase in the dissimilarity of the lattice constants, i.e., the larger their dissimilarity (the smaller the p valve), the more important is the AMM; in the converse situation, DMM is more significant. This result is in accord with the conclusions of Swartz and Pohl[4,5] (Fig. 14 of Ref. 5), but the dissimilarity cited in their paper is the difference of the product (ρc) of mass density (ρ) and the phonon velocity (c) of the two materials constituting the interface. The dissimilarity described in this paper is the difference of the lattice constant. It agrees with the findings from Schelling *et al.*'s simulation[23] that AMM dominates thermal conductivity of an interface at low frequencies, while DMM prevails at high frequencies.

Figure 2 also shows that $1/\tau(\omega)$ monotonically increases with the rise in the lattice dissimilarity parameter, p, at low frequencies, but not at high frequencies. There is a maximum at about $p \approx 50$ that can be interpreted from the Fourier transform of the displacement related to the ISF. Figure 1(b) to 1(e) reveals that the ISF becomes more long range with an increase in p; therefore, more Fourier components of long wavelengths are included in describing the lattice displacement related to the ISF. However, the Fourier components of short wavelengths of the ISF depend not only on the ISF's range, but also on the amplitude of the displacements. With their rising amplitude of displacement and the declining range of the ISF, the Fourier components of the short wavelengths increase. Although an increase in the p value extends the range of the ISF and the amplitude of the displacement [see Figs. 1(b) to 1(e)], their extensions are not equal. For example, when p tends to infinity, the range of the strain field is infinite, as is that of a single dislocation, but the amplitude is finite (excluding the dislocation core). The balance between the range and amplitude of the displacements of ISF generates an interface that can maximally scatter high-frequency phonons. To clarify the physics underlying this phenomenon, we consider two extreme cases. According to Merwe's model,[21] as $p \to 0$, the interface becomes completely mismatched. The thickness of

TABLE I. Fitting parameters.

The amount of dissimilar lattice (p)	C $(\times 10^{11})$	ω_0/ω_D
10a	1.85	0.43
20a	1.58	0.21
50a	2.31	0.08
100a	1.81	0.04
200a	1.15	0.02

the ISF will vanish, and all phonons will be transparent to it if we consider only scattering from the ISF. Conversely, as $p \to \infty$, the interface is perfectly matched, the density of the dislocation at the interface falls to zero, and, therefore, phonon scattering will disappear. Because these two extreme cases extinguish phonon scattering from the ISF, mathematical knowledge tells us that there is at least one extreme point between the two.

The temperature dependence of thermal conductivity can be governed by the frequency and temperature-dependent relaxation time of the phonon $\tau(\omega)$, as Klemens suggested.[12] Since different types of lattice defects engender different forms of the frequency dependence of $\tau(\omega)$, we can draw conclusions about the nature of lattice defects from the thermal conductivity that they induce. Although Van der Merwe's interface model (Fig. 1) is based on the assumptions introduced by Peierls and Nabarro in dealing with a single dislocation, the ISF differs from the strain field of a dislocation because, unlike that of a single dislocation, it is not a long-range strain field. Therefore, the frequency and the magnitude of $\tau(\omega)$ from the ISF should differ from those of an individual dislocation that exhibits the relationship $1/\tau(\omega) \propto \omega^{12}$ (see the inset in Fig. 2; here, a linear vertical scale is used to show the nonlinear relationship of $1/\tau(\omega)$ vs ω). We fitted our calculated curve using various polynomials; the best fit is shown by the dashed lines in Fig. 2, based on $1/\tau(\omega) = C\frac{(\omega-\omega_0)^3}{\omega_D^3}$, where C is the fitting parameter; ω_D is the Debye frequency, and ω_0 is the critical frequency at which phonons are scattered from the ISF. Table I lists these fitting parameters.

As we described earlier, phonons below a critical frequency, ω_0, can pass transparently through the ISF. For example, the phonons with a frequency $\omega < 0.43\omega_D$ are not scattered by the ISF when $p = 10a$, i.e., the periodicity of the strain field is 10 times the lattice constant. At low temperatures, only low-frequency phonons are excited, so the thermal resistance of the interface arises mainly from their contribution, implying that we can ignore the effect of ISF on thermal conductivity at low temperatures. The two general models, AMM and DMM, work well for solid-solid interfaces at low temperatures. However, at high temperatures, the influence of the ISF probably cannot be ignored since the scattering of high-frequency phonons from the ISF is stronger than that of low-frequency phonons. To assess this influence, the thermal conductivities of the interface with and without the ISF are calculated at various temperatures. According to Callaway's thermal conductivity theory,[24] the total relaxation $\tau_{\text{tot}}(q)$ is expressed as

$$\frac{1}{\tau_{\text{tot}}(q)} = \frac{1}{\tau_1(q)} + \frac{1}{\tau_2(q)} + \cdots, \tag{30}$$

where $\tau_1(q)$ and $\tau_2(q)$ are the relaxation time of different phonon scattering processes. Substituting Eq. (30) into Eq. (19), and only keep two scattering processes, the total thermal conductivity is

$$\kappa_{\text{tot}}(T) = \sum_{\omega_q} \frac{1}{\frac{1}{\kappa_1(\omega_q,T)} + \frac{1}{\kappa_2(\omega_q,T)}}, \tag{31}$$

where $\kappa_i = C(\omega_q)v^2\tau_i(q)$ $(i = 1, 2)$. Here, κ_1 represents thermal conductivity of ISF, and κ_2 is the thermal conductivity of the AMM or the DMM prediction. If we exclude the thermal conductivity from the ISF, the $\frac{1}{\kappa_1(\omega_q,T)}$ part of the denominator in Eq. (30) is eliminated, and we obtain the thermal conductivity of the pure AMM or DMM prediction, i.e., $\kappa_{\text{AMM}}(T)$ or $\kappa_{\text{DMM}}(T)$. Figure 3(a) and 3(b), respectively, shows the calculated thermal conductivity that excludes and includes the ISF of various p values. Figure 3(c) and 3(d) depicts the relative difference in thermal conductivity excluding or including the ISF for various values of the lattice-dissimilarity parameter, p. They clearly indicate that we can ignore the effect of ISF on thermal conductivity at low temperatures, but that the ISF effectively lowers the thermal conductivity of the interface at high temperatures. The reductions at 300 K are about 6–30% for the AMM prediction and 3–19% for the DMM prediction, both of which depend upon the p values. Usually, the DMM can more realistically describe the thermal conductivity of the interface at high temperatures. Therefore, the correction in thermal conductivity from the ISF is about 10%. We think these results are realistic. First, whether we use the AMM or the DMM to calculate the thermal conductivity of a solid-solid interface, the theoretical estimate is close to the experimental measurements, especially at low temperatures.[5] Second, Costescu *et al.*'s experiment[25] indicates that the 8% in-plane lattice mismatch between TiN(111) and Al_2O_3 (0001)—and the interface stacking faults in the TiN/MgO(111) and TiN/Al_2O_3 samples—does not entail a large change in the thermal conductivity at the interface. All these findings imply that the effect of ISF does not dominate the thermal conductivity of the interface; however, it can induce an ∼10% margin of error based on the AMM or DMM prediction at high temperatures. Costescu *et al.*[25] offered two possible interpretations of their observations without theoretical calculations: (1) The interfacial disorder produces strong phonon scattering at the interface, and therefore satisfies the assumptions of DMM; and (2) the interface disorder is weak; hence, phonon scattering is weak, and then the transmission coefficient always is close to unity. Our calculations imply that their second interpretation is the more reasonable if the disorder arises from the strain of interfacial lattice mismatch.

Next, we discuss experimental observations based on the results from our calculations. Precipitation is a common means by which to obtain low thermal conductivity in thermoelectric materials. Further, experiments suggest that nanostructural precipitates are very effective in scattering phonons;[26,27] several factors modulate its effectiveness. Firstly, a large compositional difference between two sides of an interface entails a large acoustic mismatch that helps to enhance acoustic phonon scattering.[4,5] The compositional contrast created by a precipitate is larger than that caused by spinodal decomposition, and, therefore, acoustic scattering in the process of precipitation is stronger than that in spinodal decomposition. Secondly, nanoscale precipitates may be more effective than nonnanoscale precipitates due to the more extensive interfacial strain regions in the former. Furthermore, a moderately coherent interface enhances phonon scattering. The interfaces between nanostructural precipitates and matrix created by a nucleation process usually preserve a better interfacial lattice coherence than that between nonnanoscale precipitates and matrix, and even more so for interfaces with a

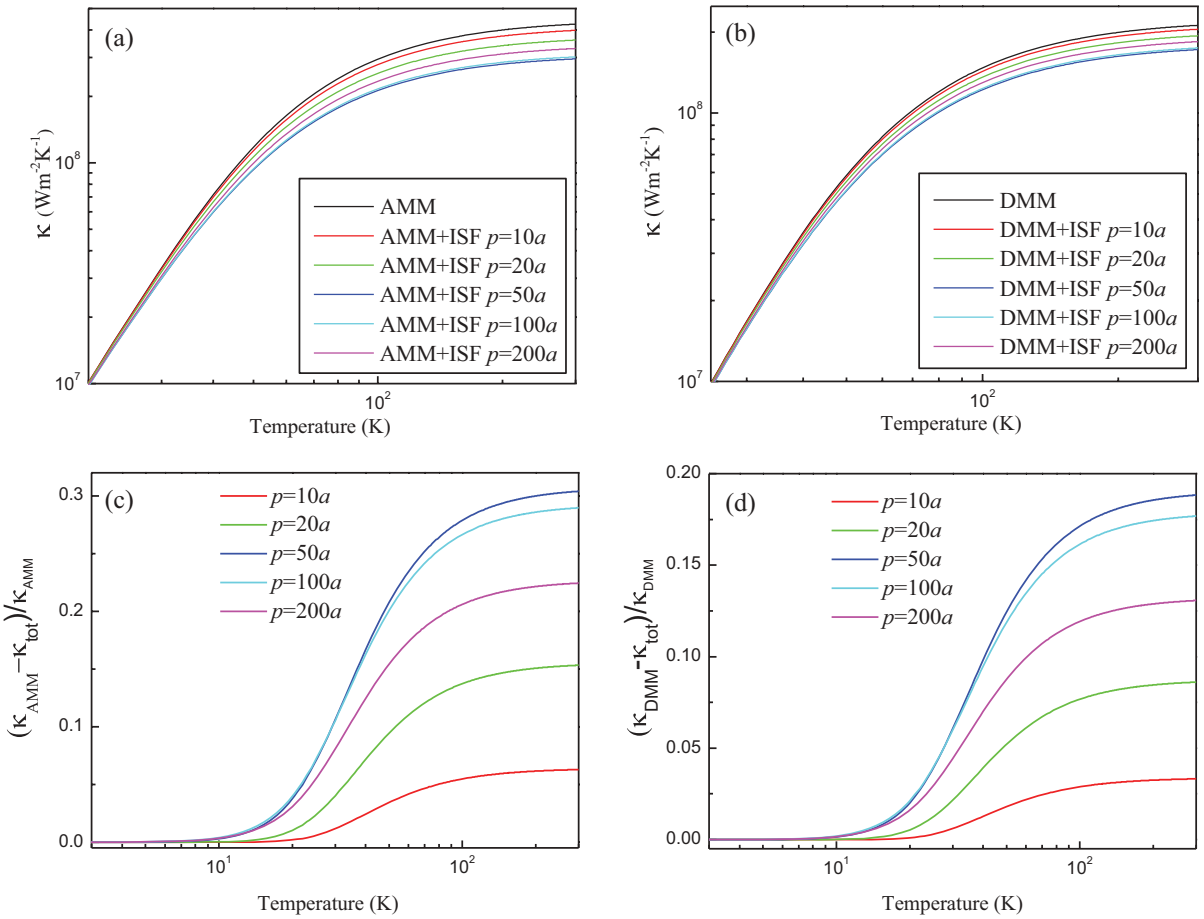

FIG. 3. (Color online) (a) Thermal conductivity of AMM (acoustic mismatch model) and AMM + ISF (interfacial strain field) with various misfit p values. (b) Thermal conductivity of DMM (diffusive mismatch model) and DMM + ISF with various p values. (c) and (d) show the relative differences with ISF and without ISF.

large lattice mismatch. Since the coherent interfaces not only have larger atomic displacement, but also a longer range of strain field than the incoherent interfaces, the former entails more effective phonon scattering.

The findings from our investigation also serve to illustrate phonon scattering from a strain field of grain boundaries. We define a grain boundary in a polycrystalline material as an interface formed by two identical lattices rotating along a common axis with a defined angle. We can use one or more sets of interfacial dislocation arrays to model the misorientation and the associated ISF of a grain boundary.[28] For a pure tilt boundary, its strain field is similar to Van der Merwe's interfacial strain field, i.e., the strain declines exponentially with increasing distance from the grain boundary, and the trend of the exponential decay depends on the periodicity of the dislocation array.[28] Low-angle pure tilt grain boundaries contain large-spaced dislocation arrays, and, therefore, the range of strain field of low-angle tilt grain boundaries is larger than that of high-angle boundaries; however, the local lattice displacement of the former is less than that of the latter. Our calculation indicates that both the range and amplitude of the strain field determine the magnitude of phonon scattering, and their competition can lead to an optimized phonon scattering for grain boundaries. Since the integration of the amplitude and range of ISF can be related to the grain boundary energy, such energy probably scales the competition, i.e., the larger the energy of the grain boundary, the more effective is phonon scattering from the grain boundary's strain field, in agreement with Schelling *et al.*'s simulation.[23]

IV. CONCLUSIONS

Our theoretical work indicates that phonon scattering from the interface strain field (ISF) rapidly weakens with a decrease in phonon frequency; below the critical frequency ω_0, there is no scattering, since the range of the ISF diminishes exponentially with the increasing extent of lattice mismatch of the two lattices making up the interface. This finding implies that phonon scattering of low frequency from the ISF contributes little to reducing the thermal conductivity at the interface. Here, the AMM is the main mechanism controlling interfacial thermal conductivity. For high-frequency phonons, i.e., as phonon wavelength approaches the thickness of the ISF, the DMM becomes progressively useful in predicting interfacial thermal conductivity, and the effect of the ISF becomes predominant.

The frequency dependence of relaxation time $\tau(\omega)$ arising from the ISF is $1/\tau(\omega) \propto (\omega - \omega_0)^3$. The critical frequency

increases rapidly with increase of the lattice misfit between the two dissimilar lattices comprising the interface. Our calculations indicate that a moderately coherent interface can more efficiently enhance phonon scattering, implying that interfaces and grain boundaries with better interfacial lattice coherence have lower thermal conductivity.

ACKNOWLEDGMENTS

The work was supported by US Department of Energy, Office of Basic Energy Science, Division of Materials Science and Engineering under Contract No. DE-AC02-98CH10886. Qingping Meng acknowledges Chinese National Natural Science Foundation (No. 50471014) for partial support and Q. Li for helpful discussions.

APPENDIX

The expressions of Eq. (29) in fcc and bcc

(1) Fcc

$$
\begin{aligned}
S = {} & \tfrac{1}{8}a^3 u_{q'-q}\left[\left(\hat{e}_q^x + \hat{e}_q^y\right)\left(\hat{e}_{q'}^x + \hat{e}_{q'}^y\right)(F_{x+y} - F_{x+y}^*) + \left(\hat{e}_q^x - \hat{e}_q^y\right)\left(\hat{e}_{q'}^x - \hat{e}_{q'}^y\right)(F_{x-y} - F_{x-y}^*)\right] \\
& + \tfrac{1}{8}a^3 w_{q'-q}\left[\left(\hat{e}_q^y + \hat{e}_q^z\right)\left(\hat{e}_{q'}^y + \hat{e}_{q'}^z\right)(F_{y+z} - F_{y+z}^*) + \left(\hat{e}_q^y - \hat{e}_q^z\right)\left(\hat{e}_{q'}^y - \hat{e}_{q'}^z\right)(F_{y-z} - F_{y-z}^*)\right] \\
& + \tfrac{1}{8}a^3(u_{q'-q} + w_{q'-q})\left(\hat{e}_q^z + \hat{e}_q^x\right)\left(\hat{e}_{q'}^z + \hat{e}_{q'}^x\right)(F_{z+x} - F_{z+x}^*) + \tfrac{1}{8}a^3(u_{q'-q} - w_{q'-q})\left(\hat{e}_q^z - \hat{e}_q^x\right)\left(\hat{e}_{q'}^z - \hat{e}_{q'}^x\right)(F_{z-x} - F_{z-x}^*),
\end{aligned}
$$

where

$$
\begin{aligned}
F_{x+y} &= (1 - e^{-\frac{1}{2}i(q_x+q_y)a})(1 - e^{\frac{1}{2}i(q'_x+q'_y)a})(1 - e^{\frac{1}{2}i(q'_x+q'_y-q_x-q_y)a}) \\
F_{x-y} &= (1 - e^{-\frac{1}{2}i(q_x-q_y)a})(1 - e^{\frac{1}{2}i(q'_x-q'_y)a})(1 - e^{\frac{1}{2}i(q'_x-q'_y-q_x+q_y)a}).
\end{aligned}
$$

F_{y+z}, F_{y-z}, F_{z+x}, and F_{z-x} are obtained by cyclic permutation of the subscripts; the superscript character "*" represents the conjugate complex. $\hat{e}_q^i$ is the directional cosine of the wave vector q.

(2) Bcc

$$
\begin{aligned}
S = {} & \tfrac{1}{8}a^3(u_{q'-q} + w_{q'-q})\left(\hat{e}_q^x + \hat{e}_q^y + \hat{e}_q^z\right)\left(\hat{e}_{q'}^x + \hat{e}_{q'}^y + \hat{e}_{q'}^z\right)(F_{x+y+z} - F_{x+y+z}^*) \\
& + \tfrac{1}{8}a^3(u_{q'-q} + w_{q'-q})\left(\hat{e}_q^x - \hat{e}_q^y + \hat{e}_q^z\right)\left(\hat{e}_{q'}^x - \hat{e}_{q'}^y + \hat{e}_{q'}^z\right)(F_{x-y+z} - F_{x-y+z}^*) \\
& + \tfrac{1}{8}a^3(u_{q'-q} - w_{q'-q})\left(\hat{e}_q^x + \hat{e}_q^y - \hat{e}_q^z\right)\left(\hat{e}_{q'}^x + \hat{e}_{q'}^y - \hat{e}_{q'}^z\right)(F_{x+y-z} - F_{x+y-z}^*) \\
& + \tfrac{1}{8}a^3(-u_{q'-q} + w_{q'-q})\left(-\hat{e}_q^x + \hat{e}_q^y + \hat{e}_q^z\right)\left(-\hat{e}_{q'}^x + \hat{e}_{q'}^y + \hat{e}_{q'}^z\right)(F_{-x+y+z} - F_{-x+y+z}^*),
\end{aligned}
$$

where

$$
\begin{aligned}
F_{x+y+z} &= (1 - e^{-\frac{1}{2}i(q_x+q_y+q_z)a})(1 - e^{\frac{1}{2}i(q'_x+q'_y+q'_z)a})(1 - e^{\frac{1}{2}i(q'_x+q'_y+q'_z-q_x-q_y-q_z)a}) \\
F_{x-y+z} &= (1 - e^{-\frac{1}{2}i(q_x-q_y+q_z)a})(1 - e^{\frac{1}{2}i(q'_x-q'_y+q'_z)a})(1 - e^{\frac{1}{2}i(q'_x-q'_y+q'_z-q_x+q_y-q_z)a}) \\
F_{x+y-z} &= (1 - e^{-\frac{1}{2}i(q_x+q_y-q_z)a})(1 - e^{\frac{1}{2}i(q'_x+q'_y-q'_z)a})(1 - e^{\frac{1}{2}i(q'_x+q'_y-q'_z-q_x-q_y+q_z)a}) \\
F_{-x+y+z} &= (1 - e^{-\frac{1}{2}i(-q_x+q_y+q_z)a})(1 - e^{\frac{1}{2}i(-q'_x+q'_y+q'_z)a})(1 - e^{\frac{1}{2}i(-q'_x+q'_y+q'_z+q_x-q_y-q_z)a}).
\end{aligned}
$$

*Corresponding author: zhu@bnl.gov

[1] D. G. Cahill, W. K. Ford, K. E. Goodson, G. D. Mahan, A. Majumdar, H. J. Maris, R. Merlin, and S. R. Phillpot, J. Appl. Phys. **93**, 793 (2003).

[2] P. L. Kapitza, J. Phys. USSR **4**, 181 (1941).

[3] W. A. Little, Can. J. Phys. **37**, 334 (1959).

[4] E. T. Swartz and P. O. Pohl, Appl. Phys. Lett. **51**, 2200 (1987).

[5] E. T. Swartz and P. O. Pohl, Rev. Mod. Phys. **61**, 605 (1989).

[6] Ch. Steinbrüchel, Z. Phys. B **24**, 293 (1976).

[7] M. E. Lumpkin, W. M. Saslow, and W. M. Visscher, Phys. Rev. B **17**, 4295 (1978).

[8] B. V. Paranjape, N. Arimitsu, and E. S. Krebes, J. Appl. Phys. **61**, 888 (1987).

[9] D. A. Young and H. J. Maris, Phys. Rev. B **40**, 3685 (1989).

[10] R. J. Stoner and H. J. Maris, Phys. Rev. B **48**, 16373 (1993).

[11] S. Pettersson and G. D. Mahan, Phys. Rev. B **42**, 7386 (1990).

[12] P. G. Klemans, in *Solid-State Physics*, edited by F. Seitz and D. Turnbull, Vol. 7 (Academic Press, Inc., New York, 1958), p. 1.

[13] P. Carruthers, Rev. Mod. Phys. **33**, 92 (1961).

[14] J. D. Eshelby, in *Solid-State Physics*, edited by F. Seitz and D. Turnbull, Vol. 3 (Academic Press, Inc., New York, 1955), pp. 79–144.

[15] R. C. Cammarata and K. Sieradzki, Phys. Rev. Lett. **62**, 2005 (1989).

[16] W. Pompe, X. Gong, Z. Suo, and J. S. Speck, J. Appl. Phys. **74**, 6012 (1993).

[17] D. Su, Q. Meng, M.-G. Han, C. A. F. Vaz, Y. Segal, F. J. Walker, M. Sawicki, Ch. Broadbridge, and Ch. H. Ahn, Appl. Phys. Lett. **99**, 102902 (2011).

[18] S. C. Jain, A. H. Harker, and R. A. Cowley, Phil. Mag. A **75**, 1461 (1997).

[19]L. Schiff, *Quantum Mechanics*, 3rd ed. (McGraw-Hill Book Company, Inc., New York, 1968), p. 285.
[20]F. C. Frank and J. H. van der Merwe, Proc. R. Soc. Lond. A **198**, 205 (1949); **198**, 216 (1949); **200**, 125 (1950); **201**, 261 (1950).
[21]J. H. van der Merwe, Proc. Phys. Soc. A **63**, 616 (1950).
[22]P. Sheng, *Introduction to Wave Scattering Localization and Mesoscopic Phenomena*, 2nd ed. (Springer, Berlin, Heidelberg, New York, 2006).
[23]P. K. Schelling, S. R. Phillpot, and P. Keblinski, J. Appl. Phys. **95**, 6082 (2004).
[24]J. Callaway, Phys. Rev. **113**, 1046 (1959).
[25]R. M. Costescu, M. A. Wall, and D. G. Cahill, Phys. Rev. B **67**, 054302 (2003).
[26]K. Biswas, J. He, I. D. Blum, Ch.-I Wu, T. P. Hogan, D. N. Seidman, V. P. Dravid, and M. G. Kanatzidis, Nature **489**, 414 (2012).
[27]J. Androulakis, C. Lin, H. Kong, C. Uher, C. Wu, T. Hogan, B. A. Cook, T. Caillat, K. M. Paraskevopoulos, and M. G. Kanatzidis, J. Am. Chem. Soc. **129**, 9780 (2007).
[28]J. P. Hirth and J. Lothe, *Theory of Dislocations* (Wiley, New York, 1982).